Dynamics of the *E. coli* β clamp dimer interface and its influence on DNA loading

Bilyana N. Koleva1, Hatice Gokcan2, Alessandro A. Rizzo3, Socheata Lim3, Kevin Jeanne Dit Fouque4, Angelina Choy1, Melissa L. Liriano1, Francisco Fernandez-Lima4, Dmitry M. Korzhnev3, G. Andrés Cisneros2 and Penny J. Beuning1,*

1Department of Chemistry & Chemical Biology, Northeastern University, Boston, MA 02115, USA
2Department of Chemistry, University of North Texas, Denton, Texas, USA
3Department of Molecular Biology and Biophysics, University of Connecticut Health Center, Farmington,
Connecticut, USA
4Department of Chemistry and Biochemistry, Florida International University, Miami, FL 33199, USA.

*To whom correspondence should be addressed. Tel: +1-617-373-2865; Fax: +1-617-373-8795; Email:
beuning@neu.edu

ORCID: 0000-0002-1283-4390 (FFL); 0000-0001-6629-3430 (GAC); 0000-0002-7770-022X (PJB)
Running title: *E. coli* beta clamp dynamics

Abstract
The ring-shaped sliding clamp proteins have crucial roles in the regulation of DNA replication, recombination, and repair in all organisms. We previously showed that the *E. coli* β clamp is dynamic in solution, transiently visiting conformational states in which domain I at the dimer interface is more flexible and prone to unfolding. This work aims to understand how the stability of the dimer interface influences clamp opening dynamics and clamp loading by designing and characterizing stabilizing and destabilizing mutations in the clamp. The variants with stabilizing mutations conferred similar or increased thermostability and had similar quaternary structure as compared to WT. These variants stimulated the ATPase function of the clamp loader, complemented cell growth of a temperature-sensitive strain, and were successfully loaded onto a DNA substrate. The L82D and L82E I272A variants with purported destabilizing mutations had decreased thermostability, did not complement the growth of a temperature-sensitive strain, and had weakened dimerization as determined by native TIMS-MS. The β L82E variant had a reduced melting temperature, but dimerized and complemented growth of a temperature-sensitive strain. All three clamps with destabilizing mutations had perturbed loading on DNA. Molecular dynamics simulations indicate altered hydrogen bonding patterns at the dimer interface and cross-correlation analysis showed the largest perturbations in the destabilized variants, consistent with the observed change in the conformations and functions of these clamps.

Introduction

The ring-shaped sliding processivity clamp protein of the DNA replication machinery has crucial roles in the regulation of DNA replication, recombination, and repair in all living organisms and some viruses. DNA polymerases replicate the genomes of entire organisms and the sliding processivity clamp provides the speed and processivity required by DNA polymerases for efficient DNA replication (1-3). The sliding clamp binds the polymerase and tethers it to DNA, allowing the polymerase to replicate DNA without dissociation from the template. Structural studies reveal that sliding clamps have a pseudo six-fold symmetry and individual subunits are arranged in a head-to-tail conformation (1, 4-8). Clamps from bacterial species (4) are homodimeric with three domains in each monomer whereas eukaryotic and archaeal species (5, 9-11) are trimers with two domains in each monomer. Each domain consists of two α- helices and two, four-stranded antiparallel β sheets; adjacent α-helices and a long curved β sheet provide the interdomain interactions (Fig. 1). The *E. coli* β clamp increases the processivity and speed of replication by ~5,000-fold and 100-fold, respectively (12-15). Clamp proteins slide on DNA and serve as platforms for multiple proteins to bind. The β clamp interacts with all five *E. coli* DNA polymerases (16- 26) and coordinates the polymerase switch during translesion synthesis (27-29). In addition, β interacts with replication initiation factors DnaA (30) and Had (31); mismatch repair proteins MutS and MutL; and DNA ligase A, which is responsible for Okazaki fragment maturation (16). Client interactions occur on the front face of the clamp at the 3′ recessed end of DNA at primer:template junctions. Clamps are loaded on DNA by clamp loader complexes, which are members of the AAA+ family ATPases (32-35). The loader functions as a switch (36, 37) and first binds ATP in order to bind to the clamp; ATP hydrolysis is not needed for clamp opening but rather for the clamp loader ejection from the clamp and DNA (38, 39). The *E. coli* clamp loader, the γ complex, contains one copy of each δ and δ′ and three copies of γ or τ subunits. The γ/τ subunits harbor the ATPase function and once ATP-binding sites are occupied, a spiral arrangement is triggered that complements the right-handed helix of DNA. The rearrangement of the clamp loader exposes a region of the δ subunit previously occluded by δ′ and allows binding of δ to the β clamp and the primer:template DNA (40). Available structural data of the γ clamp loader complex in its inactive state shows an asymmetric conformation and the steric clashes precluding it from binding the clamp (40). The structure of the γ complex bound to DNA demonstrates the active conformation of a symmetrically aligned clamp loader with all three ATP-binding sites occupied, elucidating the mechanism of ATP hydrolysis induced by γ complex binding DNA (41). The stability of clamps as closed structures varies in different organisms and trimers tend to be less stable than dimers (42-45). The ability of a clamp loader to open a clamp is determined by the stability of the clamp ring structure. The T4 bacteriophage clamp gp45 tends to be open in solution and unload readily from DNA as a trimer and monomerize (42-46), eliminating the need for the clamp loader gp44/62 to open the clamp. Heterotrimeric *Sulfolobus solfataricus* PCNA samples ring-open states in solution in the absence of its loader (47). The human clamp PCNA is less stable in solution than its nearly-identical structural homolog from *S. cerevisiae* (48). Evidence exists both for and against opening of yeast PCNA by its Replication Factor C (RFC) loader complex. It has been shown experimentally that PCNA opening is enhanced by ~20,000 fold when bound to the RFC complex compared to unbound PCNA (49-52). However, computational modeling of a mutated RFC that is unable to form a spiral arrangement appears to stabilize the open conformation of PCNA rather than destabilize its closed conformation (53). Human PCNA and the β clamp have been shown to dissociate slowly from DNA, with 1/2 of 24 and 60 min, respectively (42). The β clamp forms a dimer with a *K*D of 65-~600 pM, at a concentration three orders of magnitude lower than yeast

PCNA (52, 54), making the β clamp the most stable clamp in solution and suggesting the need for clamp opening by the clamp loader. Other work indicates that domain I at the dimer interface can undergo local unfolding in solution, suggesting that at least transient spontaneous opening is possible (55, 56).

In dimeric β, the helix harboring residues I272 and L273 of Domain III is unwound and distorted to facilitate a hydrophobic interaction with Domain I of the other β monomer to create a well-packed dimer interface (Fig. 1). The crystal structure of a monomeric β clamp (β I272A L273A) bound to the δ subunit of the γ complex reveals that this helix is undistorted, and the formation of a well-packed dimer interface is prevented (57). In addition, a five-residue loop (274-278) that is part of a turn in the dimeric β structure and therefore occluded from interaction with δ in the closed clamp provides an interaction surface for δ and monomeric β (57). Although δ does not directly interact with the dimer interface of closed β, the above rearrangements are attributed to the interaction of δ with monomeric β. The δ subunit does not open β at the dimer interface but rather stabilizes one monomer, preventing ring closure. The strained conformation of the clamp monomers held together by interactions at the dimer interface can provide the energy for δ to induce β to open or trap β in an open conformation. The monomeric β shows greater flexibility in solution compared to the dimeric structure in hydrogen-deuterium exchange mass spectrometry experiments (55) and this dynamic behavior is confirmed by steered molecular dynamics (MD) simulations (58). The simulated monomeric β is dynamic and opens more in solution relative to the dimer. The tilt observed in Domain III relative to the other domains of the monomeric clamp is the same as in the crystal structure of the monomeric β:δ complex. Fluorescence-based experiments show that clamp binding is fast while clamp opening is a slower process that does not require ATP hydrolysis (39).

The δ subunit alone or the γ complex depleted of ATP has been shown to unload dimeric β *in vitro* (59). Binding to δ stabilizes the open conformation, shifting the equilibrium between closed and open β toward an open conformation (57, 58).

We previously found that the β clamp undergoes opening transitions in solution and occupies conformational states in which Domain I of β is particularly dynamic, undergoing local cooperative unfolding (55, 56). These findings along with other work demonstrating that β is flexible and under tension in the dimeric state suggest that β may transiently sample multiple conformations, some of which could be more favorable for clamp loader binding. The goal of this study is to better understand how the stability of the β clamp dimer interface influences its dynamic properties and the opening and closing of its ring structure underlying clamp loading. We made a broad set of mutations aimed at stabilizing the closed conformation or destabilizing the dimer interface. Biochemical, biophysical, and computational analyses reveal correlations between dimer stability and clamp opening and loading functions of the β clamp variants.

Experimental Section

Protein Expression and Purification

The *dnaN* gene encoding the β clamp was previously cloned into pET11T and expressed and purified generally as described (55). Detailed methods can be found in the Supporting Information. Mutations in this construct were introduced using the QuikChange II Site-Directed Mutagenesis Kit (Agilent Technologies, Santa Clara, CA). Mutations were confirmed by DNA sequencing (Eton, Charlestown, MA). The γ clamp loader complex was expressed and purified as previously described (41). For isothermal titration calorimetry (ITC) experiments, the *dnaN*

gene and a fragment of the *holA* gene encoding the N-terminal domain of the *E. coli* γ clamp loader complex d subunit (residues 1-140; referred to as mini-δ) were subcloned into the pET28b+ vector (Novagen, Darmstadt, Germany) using the NdeI and XhoI sites, as described elsewhere (60). Point mutations in the β-clamp gene, including T45R, T47R, S107R, S109R, L82D, L82E, L82E I272A, and I272A L273A were introduced following the modified inverse PCR procedure (61). The nucleotide sequence of the resulting constructs was confirmed by sequencing (Genewiz, Cambridge, MA). Recombinant mini-δ, WT β, and variant β clamps T45R, T47R, S107R, S109R, L82E, L82E I272A, and I272A L273A were expressed and purified as described previously (60), and in the Supporting Information. The β clamp L82D variant could not be purified in sufficient amounts for ITC experiments.
To test for a potential interaction between β and SSB, *E. coli* BL21(DE3) strain containing pEAW134 (a gift from Dr. Michael Cox from the University of Wisconsin, Madison) expressing single-stranded DNA binding protein (SSB) (62) was transformed with pET28b expressing His-tagged β clamp. Transformants were selected on LB plates supplemented with ampicillin and kanamycin. A 50-mL starter culture in a shake flask (200 rpm) was grown overnight at 37 °C. A 1-L culture was seeded and grown at 37 °C until OD600 of 1.0 was reached. Protein expression was induced with IPTG to a final concentration of 1 mM at 30 °C for 4 h. Cells were harvested by centrifugation for 10 min at 6,750 × g at 4 °C and frozen at -80 °C or lysed immediately. Protein overexpression was confirmed by SDS-PAGE analysis. Affinity chromatography was used to investigate possible β and SSB interactions (63, 64). Cell pellets containing overexpressed β and SSB were resuspended on ice in 50 mM HEPES, pH 7.5, 500 mM NaCl, 30 mM imidazole, 1 mM DTT, 15% glycerol (Buffer A) supplemented with lysozyme and +/- DNase I. Cells were lysed by repeated freeze/thaw cycles (-80 °C followed by 37 °C). Cell debris was pelleted by centrifugation at 14,000 × g at 4 °C for 1 h. The lysate was loaded onto a 2 × 5 mL HisTrap HP (GE Healthcare, Marlborough, MA) column and eluted with Buffer A and increasing imidazole concentration to 0.5 M. Fractions were analyzed by SDS-PAGE.

Differential Scanning Fluorimetry (DSF)
The melting temperature of the WT and variant β clamps was determined using a thermofluor-based assay (56, 65). Optical 96-well clear PCR plates (Fisher) were used to analyze the melting temperature (Tm) of β proteins. Samples containing 5 μM β protein and a final concentration of 10x Sypro Orange dye (Invitrogen, Carlsbad, CA) were prepared in a 20-μL reaction volume containing 20 mM HEPES, pH 7.5. The plates were sealed with an optical adhesive film (Applied Biosystems, Foster City, CA). The temperature in a CFX 96 Real-Time System (Bio-Rad, Hercules, CA) was raised from 4 °C to 100 °C in 0.2 °C increments every 10 s and the fluorescence was detected. Samples were analyzed three times in duplicate and average Tm and standard deviations are reported.

Native and denaturing PAGE
Purified WT β and variants (1 μg each) were incubated in 1x loading buffer (62.5 mM Tris-HCl, pH 6.8, 0.01% Bromophenol Blue, 2.5% βME, 10% glycerol) prior to loading onto 12% PAGErTM precast gels (Lonza. Basel, Switzerland) for native PAGE. Proteins were incubated in loading buffer supplemented with 2% SDS at 95 °C for 10 min prior to loading on 16% SDS-PAGE. Gels were stained with Coomassie gel stain.

Native nESI-Trapped Ion Mobility Spectrometry – Mass Spectrometry (TIMS-MS)

Ion mobility – mass spectrometry experiments were performed on a custom built nESI-TIMS unit coupled to an Impact Q-TOF mass spectrometer (Bruker, Billerica, MA) (66, 67). The TIMS unit is run by custom software in LabView (National Instruments, Austin, TX) synchronized with the MS platform controls (67). Aliquots (10 mL) of WT and clamp variants, dissolved in 10 mM NH4Ac (native conditions) to 5 μM, were loaded in a pulled-tip capillary biased at 1500 V to the MS inlet. Briefly, the ion mobility separation in a TIMS device is based on holding the ions stationary using an electric field (*E*) against a moving buffer gas (68). TIMS separation depends on the gas flow velocity (*vg*), elution voltage (*Velution*), ramp time (*tramp*) and base voltage (*Vout*) (66). The mobility, *K*, is defined by:

$$K = \frac{v_g}{E} \cong \frac{A}{(V_{elution} - V_{out})} \quad (1)$$

The mobility calibration was performed by varying the ramp time in order to determine Velution as described (69). The mobility calibration constant *A* was determined using known reduced mobilities of Tuning Mix components from Agilent (Santa Clara, CA) analyzed under the same experimental conditions. TIMS experiments were carried out using nitrogen (N2) as a buffer gas at ambient temperature (*T*) with *vg* set by the pressure difference between the funnel entrance (P1 = 2.6 mbar) and exit (P2 = 1.1 mbar). An rf voltage of 200 Vpp at 880 kHz was applied to all electrodes. Ions were softly transferred and injected into the TIMS analyzer section injection to avoid collisional induced activation (i.e., Vdeflector = 80 V, Vcapillary= 70V, Vfunnel in = 0 V and Vout = 60 V; TIMS cell schematic shown in Fig. S1). The measured mobilities were converted into collision cross sections (CCS, Å²) using the Mason-Schamp equation:

$$\Omega = \frac{(18\pi)^{1/2}}{16} \frac{q}{(k_B T)^{1/2}} \left(\frac{1}{m} + \frac{1}{M}\right)^{1/2} \frac{1}{N} \times \frac{1}{K} \quad (2)$$

where *q* is the ion charge, *kB* is the Boltzmann constant, *N* is the gas number density, *m* is the ion mass,
and *M* is the gas molecule mass (68).

Isothermal titration calorimetry (ITC)

The interaction between the WT β or variant clamps with mini-δ was analyzed by ITC performed at 25 °C (20 °C for L82E, L82E I272A, and I272A L273A β variants) on a Nano-ITC (TA Instruments, New Castle, DE). The ITC experiment consisted of 20 x 2.5 μL injections of mini-δ (0.6 – 0.7 mM) to the β clamp solution (0.1 mM) repeated with 300 s interval between injections. The ITC data were corrected for heat measured in corresponding blank titrations of mini-δ into buffer. The data were analyzed using the NanoAnalyze software (TA Instruments) to obtain the dissociation constant *K*D, association enthalpy _H, and binding stoichiometry parameter n.

ATPase assay and Clamp loading assay
The ATPase assay was performed as per the BIOMOL® Green manual (Enzo Life Sciences, Farmingdale, NY). The clamp loading assay was carried out by separating biotinylated-DNA-

bound proteins from unbound proteins using streptavidin magnetic beads (NEB, Ipswich, MA). Both assays are described in detail in the Supporting Information.

Complementation assay

Chemically competent *E. coli* MS120 strain (70) bearing temperature-sensitive mutations in the chromosomal *dnaN* gene was transformed with pET11T empty vector (EV), plasmid encoding WT, or variant β clamp using a standard transformation procedure (71). After outgrowth at 30 °C, cells were plated on LB agar plates, in triplicate, supplemented with ampicillin and grown at 30 °C or 37 °C for 16- 18 h. Experiments were repeated three times. Average colony forming units and standard deviations are reported. Despite the likely low level of expression with pET vectors, β expressed from pET11T is found to complement a *dnaN*Ts strain and was detected by immunoblot. Indeed, we previously observed sufficient expression from a pET vector of replication protein DnaE to complement a strain harboring a temperature-sensitive allele of *dnaE* (72).

Molecular Dynamics Simulations

Seven different systems were prepared using the X-ray crystallographic structure of the *E. coli* DNA polymerase III b subunit (PDB code 1MMI) (8) containing two monomers (A and B), and subjected to MD simulations. The residues that are located on Monomer B are depicted with a prime sign. Each monomer within the proteins contains three different domains that are named alphanumerically with capital "D" and the domain numbers, D1, D2, and D3. The domains on Monomer B are indicated with a prime sign as D1′, D2′, and D3′. The topology and coordinate files were built following hydrogenation of the samples using the tLEaP module in AMBER16 (73). All of the amino acids were protonated in aqueous solution (TIP3P water) and the ff14SB force field parameters were used to model the amino acids (74). The total charge of the WT protein was -22, the total charge of the variants containing negatively charged amino acid (Asp and Glu) mutations was -24, and the total charge of the variants containing Arg mutations was -20. In order to neutralize the total negative charge of the samples, potassium counter ions were added. The waters in the crystallographic structure were deleted and the system was solvated using TIP3P water molecules. The distance between the solute and the edge of the box was chosen as 12 Å resulting in an average box dimension of 118.7 Å × 84.0 Å × 128.2 Å. All simulations were performed using the CUDA version of the Amber 16 pmemd program (73, 75, 76). Berendsen temperature coupling (77) was employed and a time step of 1.0 fs was used in all simulations. Periodic boundary conditions were imposed on the samples and the particle mesh Ewald summation technique (78) was used with 8 Å cutoff distance. SHAKE algorithm (78) was used for the bonds involving hydrogen atoms. The systems were equilibrated with an 11-stage process following a 1000-step minimization for each system. First, a 10-ps MD simulation was performed at 10 K using a harmonic restraint of 250 kcal/mol/Å2 on all residues. Second, the harmonic restraint was reduced to 100 kcal/mol/Å2 in a simulation of 10,000 steps at 10 K. In the third and the fourth stages, the harmonic restraints were reduced by half in simulations each of which were 20 ps at the same temperature. Fifth, the temperature was gradually increased to 300 K in a 10-ps simulation using a harmonic restraint of 500 kcal/mol/Å2. Sixth, a 40-ps simulation was performed at 300 K using the same harmonic restraint for all systems. Seventh, the restraints were reduced to 250 kcal/mol/Å2 in 20,000 steps simulation, which was followed by eighth, another 20,000 steps of simulation with a harmonic restraint of 100 kcal/mol/Å2 for each system. Ninth and tenth stages were performed with the same harmonic constraints as in the

third and the fourth stages, respectively, but at 300 K with 20-ps long simulations for both stages. Finally, eleventh, a 20-ps simulation was performed without harmonic restraints at 300 K. Production simulations were performed in the NVT ensemble at 300 K. Seven different MD trajectories were simulated, each of which was 100 ns.

Trajectory analysis and visualizations. Root-mean-square deviation (RMSD), root-mean-square fluctuations (RMSF) of the residues, dynamic cross-correlation analysis, and hydrogen bond analysis of the trajectories were performed using the cpptraj module (79). All three-dimensional representations were obtained using VMD (80), and the two-dimensional representations were prepared using MarvinSketch (http://www.chemaxon.com) (81).

Results

Motivations for this study and design of the β clamp variants

The ability of clamp proteins to open and close is essential to their function as protein hubs for recruitment of interacting protein partners that regulate traffic on DNA during replication and repair (2). The dimer interface of the *E. coli* β clamp is stabilized by four antiparallel β strands and two α-helices, yet there is evidence that the β clamp undergoes opening events and populates conformational states in which Domain I at the dimer interface in particular is dynamic (55). Several hydrophobic residues line the dimer interface and previous attempts to destabilize the interface to a considerable extent have proven unsuccessful except for the double mutation I272A L273A, which is a monomer at low micromolar concentrations (55, 82). The β clamp point mutation variants F104W, F106A, F106W, and L273A are dimers in solution (82-84). Newer work suggests that electrostatic interactions play a key role in stabilizing the interface (52, 54). Our goal in this work was to design and characterize mutations at the dimer interface to test the hypothesis that the clamp transiently populates open conformational states captured by the high affinity binding by the clamp loader in the process of clamp loading.

Our approach included constructing a broad range of mutations altering the stability of the dimer interface (Fig. 1). Starting with the crystal structure of the clamp (4, 8) as a guide, we chose a set of amino acid substitutions with the goal of either stabilizing or destabilizing its dimeric structure. We avoided making mutations at L273 because this residue lies on the side of the β clamp involved in binding DNA polymerases and the clamp loader and could interfere with these interactions. Furthermore, we designed mutations away from residues E93 and L98 because they are important for interactions with DinB and UmuC (26, 85-87).

To weaken the dimer interface, we introduced charge at residue L82, specifically L82D and L82E, in order to remove existing hydrophobic interactions and increase the repulsion at the dimer interface. Additionally, we combined the L82E mutation with an I272A mutation which replaces a larger hydrophobic residue with a smaller one. We hypothesized that mutating S107 and S109 to charged arginine residues would cause the formation of a salt bridge across the dimer interface and thereby stabilize the β sheet at the dimer interface. Furthermore, we wanted to stabilize Domain I of the clamp to reduce the conformational flexibility we previously observed in this region. In the hydrogen-deuterium exchange mass spectrometry (HXMS) experiments, we observed increased deuterium uptake consistent with β transiently populating open states in which Domain I is more flexible and prone to unfolding. Indeed, the peptide including residues 1-34 exhibited EX1 kinetics indicating local unfolding in that region of the clamp (55, 56). Thus, we made mutations near this region, introducing charged Arg at positions T45 and T47 in order to increase ionic interactions with E52 and stabilize β strand 4 and α-helix

1. While these mutations likely stabilize Domain I in the context of both the closed state and the open states with disrupted dimer interface, we expect they also increase stability of the β dimer by reducing the entropic penalty associated with the loss of Domain I flexibility upon formation of the closing ring.

Thermostability gives insight into the effect of dimer interface mutation

To assess whether we had altered the thermostability of the resultant variant clamps, we used a thermofluor assay, in which WT and variant β clamp proteins incubated with a fluorescent dye were subjected to increasing temperatures. Initially no fluorescent signal is observed because the fluorescence of the dye is quenched by water but as the protein denatures more of its hydrophobic regions are exposed and more dye binds until maximal fluorescent signal is reached (Fig. 2A). From this we can calculate the melting temperature of the protein which is defined as the temperature at which 50% of the protein is unfolded. A stabilizing mutation is expected to increase the melting temperature of the protein and a destabilizing mutation is expected to decrease the melting temperature. Indeed, all mutations that were designed to be stabilizing, namely T45R, T47R, S107R, and S109R, have melting temperatures similar to or a few degrees higher than WT β (69.0 °C) (Fig. 2B). Compared to WT β, β L82D and β L82E I272A have significantly lower melting temperatures of 49.5 °C and 45.3 °C, respectively, whereas the L82E mutation more modestly decreases the melting temperature to 62.3 °C. Overall, following the above strategy we have successfully designed a set of both stabilizing and destabilizing β clamp mutants that we subsequently use to correlate the β dimer stability with opening dynamics, clamp loader binding, and loading efficiency.

Native gel electrophoresis and Native nESI-TIMS-MS shows altered dimerization state of variants

A representative denaturing gel (Fig. 3A) shows the purity of WT and variant β clamps and monomeric conformations on SDS-PAGE. The dimerization state of WT and variant β clamps was evaluated by native gel electrophoresis (Fig. 3B). WT β and the T45R, T47R, S107R, and S109R variants have a pronounced dimer band whereas mutations at position L82 only or when in combination with I272A result in a less prominent dimer band. Indeed, the L82D variant shows a very weak dimer band and instead shows mainly monomeric and multimeric conformations, which are presumably monomers forming multimeric structures.

Mass spectra of the WT β clamp and the L82E variant displayed a major dimer distribution, ranging from [M+16H]16+ to [M+20H]20+ (Fig. 4A,B and Table S1), and a minor tetramer distribution, ranging from [M+25H]25+ to [M+28H]28+ and [M+24H]24+ to [M+28H]28+, respectively (Fig. 4 and Table S1), when using native nESI. In the case of the L82E I272A variant, the mass spectrum displayed an equivalent monomer and dimer distribution, ranging from [M+10H]10+ to [M+12H]12+ and [M+16H]16+ to [M+19H]19+, respectively (Fig. 4C and Table S1). However, only a monomer distribution, ranging from [M+10H]10+ to [M+12H]12+, was obtained in the MS spectrum of the L82D variant (Fig. 4D and Table S1). The present MS data were thus found consistent with our other observations indicating that the L82E I272A and L82D variants destabilize the clamp structure while the glutamic acid mutation at residue L82 (L82E) does not disrupt the clamp as much. Typical TIMS spectra for the multiply protonated species of the *n*-mers of the clamp variants are shown (Fig. 4) and the measured collision cross sections (CCS) are listed in Table S1. Inspection of the TIMS spectra for dimers and tetramers of the WT clamp exhibited higher CCS values as compared to the dimers and tetramers of the L82E variant for the same charge states. This means that the additional negative charge provided by the

L82E mutation leads to a more compact conformation than the WT clamp probably by making additional hydrogen bonds around the mutation site (see below, Molecular Dynamics simulations). In addition, the presence of some dimers for the L82E I272A variant at similar CCS values, as compared to the L82E variant dimers, suggests that the hydrogen bond network is only partially perturbed by substituting a larger hydrophobic residue by a smaller one. Furthermore, the observation of only monomers for the L82D variant at similar CCS values as compared to some monomers observed for the L82E I272A variant suggested that the two monomer variant structures adopt similar conformations despite the different mutations. The native TIMS-MS experiments enabled us to conclude that the mutation most responsible for the disruption of the dimers is provided by the negatively charged L82D, in which the hydrogen bond network is strongly perturbed around the mutation site as compared to the L82E and L82E I272A variants in the gas-phase. Our observations from native gel electrophoresis and TIMS-MS indicate that WT β, stabilizing T45R, T47R, S107R, and S109R variants, and moderately destabilizing β L82E variant remain dimeric at micromolar concentrations, while β L82E I272A and β L82D are at least partially monomeric.

Designed β variants bind mini-δ with affinity similar to that of WT β

To probe the effect of altered stability of the β clamp variants on their affinity for the clamp loader complex, we characterized interaction of mini-δ with WT β, with the stabilizing variants β T45R, β T47R, β S107R, and β S109R, and with the destabilizing variants β I272A L273A, β L82E, and β L82E I272A using ITC. Note that we were unable to express and purify the least stable variant β L82D in the amount necessary for ITC binding studies with mini-δ. The raw ITC data and the fits for the β clamp variants are hown in Fig. S2. The binding parameters for mini-δ with all considered β-clamp variants, including the equilibrium dissociation constant *K*D, association enthalpy _H, binding stoichiometry parameter n, and association entropy _S, are listed in Table 1.

Previous studies demonstrated that the equilibrium dissociation constant *K*D for δ binding to WT β (determined by SPR) is 1-2 orders of magnitude weaker than the *K*D for δ binding to β I272A L273A (82), therefore this variant was included here as a control. We were able to confirm this result by ITC (Table 1; Fig. S2): titration of mini-δ into a solution of WT β resulted in a *K*D of about 6 μM, while *K*D for mini-δ binding to β I272A L273A was 0.5 μM, over one order of magnitude stronger. Furthermore, the association enthalpy for β I272A L273A was about 1.6-fold higher than for WT β (_H of -35 kJ/mol) vs -22 kJ/mol for WT β). It is remarkable that mini-δ binding to WT β also resulted in positive (favorable) change in entropy (_S ~28 J/mol/K), presumably due to dehydration of the binding interface accompanied by an increase in solvent entropy. On the other hand, the association entropy for mini-δ binding to β I272A L273A was much smaller than for WT β (_S ~2.0 J/mol/K). This is consistent with higher flexibility of the I272A L273A β mutant, presumably due to increased sampling of a more dynamic open conformation, which is reduced upon mini-δ binding.

On the other hand, ITC analysis for mini-δ binding to stabilized β variants T45R, T47R, S107R, S109R resulted in *K*D values of 4-7 μM and _H about -20 kJ/mol, similar to those obtained for mini-δ binding to WT β. However, the association entropy for two of the stabilized variants (S107R, S109R; _S ~34-37 J/mol/K) was slightly higher than for WT β (_S ~28 J/mol/K), potentially pointing to a smaller
entropic penalty associated with a decrease in β clamp flexibility upon mini-δ binding. Interestingly, the *K*D (6.6 μM) and association enthalpy and entropy (_H ~ -18 kJ/mol, _S ~39 J/mol/K, respectively) obtained for the destabilized L82E variant are similar to those for β

S107R and β S109R, likely suggesting that at concentrations used in our ITC measurements (~100 μM) β L82E predominantly resides in the closed state. However, β L82E I272A, while displaying only a marginally stronger *K*D (5.5 μM), shows similar trends as β I272A L273A, i.e. higher association enthalpy than for WT β (_H of -34 kJ/mol vs -22 kJ/mol) and a much smaller association entropy (_S of -15.3 J/mol/K vs 28 J/mol/K). These ITC data suggest that stabilizing (T45R, T47R, S107R, S109R) and moderately destabilizing (L82E) β variants reside in the closed state at our experimental conditions (~100 μM β) and exhibit *K*D and _H for mini-δ binding similar to those observed for WT β. On the other hand, more destabilizing β L82E I272A and β I272A L273A variants increasingly populate open-like conformation(s) and exhibit larger (favorable) association enthalpy _H and smaller (less favorable) association entropy _S, which is consistent with the formation of more stabilizing intermolecular contacts and greater flexibility loss for open β clamp upon mini-δ binding.

Lower ATPase activity of the γ complex is observed in the presence of β L82D and DNA

We next assessed whether the variant β clamps stimulate the ATPase activity of the γ complex in the presence of primed DNA, using a colorimetric inorganic phosphate quantitation assay. We incubated each of the reaction components alone or in combination and measured the absorbance to assess color formation; the increase in inorganic phosphate in solution is brought about by the ATPase activity of the γ complex (Fig. 5A). No significant color change is observed when ATP, β, γ complex, or DNA alone, are incubated in assay buffer, or when ATP and γ complex or ATP, β, and γ complex are incubated in the absence of DNA. ATPase activity is detected when primer:template DNA is added to ATP, β, and the γ complex. The β L82D variant does not enhance the ATPase activity of the γ complex, β S109R shows a modest decrease in conferring enhancement of the ATPase activity, and other variants result in similar levels of ATPase activity compared to the level induced by the presence of WT β clamp (Fig. 5B). ATP hydrolysis occurs upon release of β on DNA by the γ complex, so reduced ATPase activity could be due to defects in clamp binding to the loader, clamp loading, or in release of the β clamp on DNA.

Stabilized variants are efficiently loaded onto primer:template DNA

To evaluate clamp loading of the β variants, we adapted an assay (88) utilizing a 5′ biotinylated primer:template substrate with a 5′ single-stranded overhang for loading of the clamp and streptavidincoated magnetic beads that allow for separation of bound and unbound protein. To prevent β from sliding off the linear DNA, SSB is added to the loading reactions which traps β on ssDNA (Fig. S3). After the

loading reactions are washed with buffer, bead resuspensions are applied to the magnet, the pellet (P) fractions indicate loaded β, and the supernatant (S) fractions indicate unloaded β, shown at 0 and 60 min. Representative anti-β immunoblots show the loading efficiencies of the WT and variant β clamps (Fig. 5C and S3). Overall, the amount of loaded β and the amount still present after 60 min is greater in the variant clamps with intended stabilizing mutations T45R, T47R, S107R, and S109R, as indicated by the greater amount of β in the pellet at 0 and 60 min (Fig. 5C). Less of the L82D variant is loaded on DNA than WT β; whereas the β L82E, and L82E I272A variants appear to remain loaded on DNA as indicated by the absence of β in the supernatant at 0 and 60 min and the presence of β in the pellet at 60 min. These observations could indicate altered interactions with the clamp loader and, in the case of β L82D, are consistent with a less stable β dimer. The ITC experiments (Table 1; Fig. S2), which indicate similar equilibrium dissociation constants for these clamps as for WT β binding to mini-δ, were carried out with only a truncation of the δ subunit of the clamp loader, whereas the ATPase and loading assays are carried out with the full five-subunit clamp loader. We did not observe in our

simulations that the destabilizing β variants have more extensive contacts with DNA than WT β; however, altered or additional hydrogen bonding interactions at the dimer interface could explain the persistence of the destabilizing β variants on DNA (Fig S3; see below, Molecular Dynamics simulations).

β L82D and β L82E I272A variants do not support cell growth in complementation assay

To determine whether the variant β clamps support cell growth, we utilized an *E. coli* MS120 strain (70) bearing mutations conferring temperature sensitivity in the chromosomal *dnaN* gene. The MS120 strain grows uninhibited at 30 °C but is unable to grow at temperatures of 37 °C or higher, unless complemented with a functional β gene. We transformed these cells with either empty vector or plasmids expressing WT or variant β clamps and grew them at 30 °C and 37 °C and determined the number of colony forming units at each temperature (Fig. 6). All transformants grew at 30 °C but only those that produced functional clamps were able to support growth at 37 °C. The β L82D and β L82E I272A variants did not support cell growth in the complementation assay. Interestingly, the β L82E variant was able to complement growth but the resultant colonies were much smaller, suggesting these clamps were compromised, resulting in a growth defect. Thus, all stabilizing clamp variants confer growth on the temperature-sensitive strain, whereas the destabilizing variants β L82D, β L82E I272A, and β L82E are unable or less able to rescue growth at the non-permissive temperature. We analyzed protein levels at the nonpermissive temperature by immunoblotting, which shows that the variants were expressed as detectable levels, except the L82E I272A variant, which doesn't support growth at 37 °C and therefore was not analyzed (Fig. S5).

Molecular Dynamics simulations reveal altered conformations and dynamics of β clamp variants

MD simulations with WT b clamp and the seven variants were performed to evaluate the effect of the mutations on the dynamics of the protein. The stability of the trajectories has been investigated with RMSD analysis of the backbone atoms (C, Ca, and N) of β, on Monomer A and B separately. In all cases the average RMSD for both the full-length protein and backbone atoms on Monomers A and B was at or below 3 Å (Fig. S6 and S7).

Changes in RMSF relative to WT β were determined to assess the effect of the point mutations on the fluctuations for the different variants. Nine residues with a change in relative RMSF value greater than ±1 Å were observed for the different variants (Fig. S11). P20′, L21′, and G22′ on Monomer B (indicated by the prime symbol) become more mobile in the L82E variant (Fig. S11, green) relative to WT β. D120′, which is located on the inter-domain connector loop (IDCL) between D1 and D2, becomes more mobile in the S107R variant (Fig. S11, cyan), while the mobility of D120′ is observed to be either very similar to that of the WT protein or calculated to be less than that of WT β for all other variants. The IDCL has been previously reported to have regions that are rapidly deuterated in HXMS experiments with different clamp proteins (56).

The effect of different point mutations on the correlations between the residues located at the dimer interface was studied by calculating the deviation of the cross correlations with respect to WT β (Fig. S12). Helix-3 (H3) and Helix-21 (H21) are observed to be mostly positively correlated in the L82E, T45R, and S107R variants (Fig. S12A, region colors: blue-cyan) while negative correlations are found for the remaining systems relative to WT β. For the Domain 3-Domain 1′ interface, Helix-10 (H10) and Helix-14 (H14) are observed to be correlated in the T45R and S107R variants (Fig. S12B, region colors: blue-cyan). The L82E and L82E I272A variants increase the number of residues in β sheets that are correlated with each other on the domain interface between Domain 1 and Domain 3′. The region composed of residues from L82

to R96 in particular is found to be highly correlated with the region composed of residues Y282′ to N295′ in these variants. It is noteworthy that the magnitude of the correlations between these β sheets is the highest in the L82E I272A variant relative to the other systems (see SI for detailed results).

The two-dimensional representation of the hydrogen bonds that are observed within the dimer interface based on a hydrogen bond analysis of the simulations are given in Fig. S15 where each hydrogen bond interaction is depicted by a different color. Several changes on the inter-domain contacts are observed depending on the individual mutation. The L82D and L82E variants introduce negatively charged residues into the protein, which alter the hydrogen bond network around the mutation site. The total fraction of frames that had hydrogen bonds around the mutation site is depicted in Fig. 7. It is observed that the hydrogen bond between the backbone oxygen atom of G81 and the side chain of Q265 of the neighboring monomer is conserved in both interfaces in a higher percentage of the sampled frames of β L82D, while the Domain 1-Domain 3′ interface exhibits the interaction for a higher percentage than on the Domain 3-Domain 1′ interface of the β L82E variant (Fig. 7A) relative to WT β. This interaction is conserved with a higher percentage in at least one dimer interface of β L82E I272A variant relative to WT protein (Fig. 7A). There is almost no alteration in these interactions with other mutations. In the WT protein, the backbone oxygen atom of G81 and G81′ forms a hydrogen bond with the side chain of R269′ and R269 respectively (Fig. 7B). However, the L82D variant results in a smaller total fraction of frames with this hydrogen bond present. On the other hand, the L82E variant increases the time this interaction is observed, especially on the Domain 3-Domain 1′ interface.

A similar pattern is seen in the β L82E I272A variant but with longer conservation time on the D1-D3′ interface compared with the Domain 3-Domain 1′ interface. These results indicate that the mutation of L82 to a negatively charged residue, especially Glu, increases the total fraction of time that the backbone oxygen atoms of G81 and G81′ can receive a hydrogen bond from a neighboring residue. The mutations in the T45R and S107R variants also increase the number of frames where G81 and G81′ have hydrogen bonds with R269′ and R269, respectively, relative to WT β (Fig. S15 and 7B). The most dramatic alteration observed is for the L82D, L82E, and L82E I272A variants, where a new contact is formed only in these systems and not any other. In these systems the carboxyl moiety on the sidechains (D or E) form hydrogen bonds with the positively charged side chain of R269 and R269′ (Fig. 7C and D). This interaction is maintained at least 60% of the simulation time in the β L82D variant. In the β L82E variant, the two dimer interfaces appear to be asymmetric with respect to hydrogen bonding between residues 82 and 269. The introduction of the additional mutation, I272A reduces the distinctive feature between the two dimer interfaces of β L82E I272A, in which the interactions are present at least 60% of the simulation time at both dimer interfaces. These results are consistent with the fact that this variant remains loaded on DNA. Similar differential effects at other locations in β are observed for other sites including R96 and R96′, S109 and S109′, and T45R and T45′R (see Supporting Information). As with the cross-correlation analysis, the largest perturbations to hydrogen bonding are found in the destabilizing β L82D, L82E, and L82E I272A variants.

Discussion

Structural and biochemical observations have provided many of the mechanistic details regarding the clamp loading process and reveal variations across species. The crystal structure of *E. coli* γ complex in its inactive conformation demonstrates its inability to bind to the β clamp

due to steric clashes (40). The crystal structure of the γ complex with all its ATPase sites occupied bound to DNA reveals its active conformation and the mechanism of ATP hydrolysis (41). However, the conformation of the clamp loader when it binds the clamp is unknown as the crystal structure of the clamp-clamp loader complex has not been solved, possibly because such an intermediate may be short-lived as the clamp may sample open and closed states in solution. Clamp loader-facilitated opening of the clamp can be an active process in which the clamp loader binds a closed clamp and opens it or the clamp loader can bind to and stabilize a transiently-open clamp (42-45). The T4 bacteriophage clamp gp45 is frequently open in solution and therefore does not need a dedicated clamp loader for opening; instead the gp44/62 stabilizes the open conformation (42-46). The crystal structure of the T4 gp45 clamp bound to gp44/62 clamp loader and DNA (89) reveals an open clamp-clamp loader assembly, while in the structure of the yeast PCNA-RFC complex, the clamp is closed (90). The yeast closed clamp structure may be an artifact because an arginine finger variant of the clamp loader was used that renders the loader unable to form a helical conformation and bind the clamp.

The β clamp has a t1/2 of 60 min on DNA (42). In *E. coli*, the δ subunit moderates the affinity of the complex for the clamp (91) and the δ subunit alone has been shown to unload the clamp (59). The δ subunit has been demonstrated to have a higher affinity for the β monomer rather than the dimer suggesting that δ prefers the open conformation of β (57). The structure of mini-δ bound to a β variant that is not a stable dimer shows a relaxed curvature that results in a ~15 Å opening at one dimer interface, a distortion wide enough to accommodate ssDNA (57). The δ subunit does not destabilize β at the dimer interface but rather binds to the hydrophobic pocket where most β client interactions occur (57). The helix containing residues I272 and L273 in β Domain III is under strain and allows for an inter-monomer hydrophobic interaction with Domain I, forming a tight dimer interface. In the crystal structure of the monomeric β clamp bound to the δ subunit, these residues are mutated to alanine and these smaller hydrophobic residues prevent dimer formation in the low micromolar range (57). Furthermore, the five residue loop immediately following those residues provides an interaction surface for monomeric β and δ while the loop is occluded in dimeric β. The monomer shows more dynamic behavior than WT β in the HXMS experiments (55). This greater flexibility is supported by steered MD simulations as the monomer opens up more relative to the dimer (58) and this region is perturbed most in the β L83E variant (Fig. S11). A 7° interdomain angle is observed in the simulated monomeric clamp (58) which is similar to the angle observed in the crystal structure of the β monomer complexed to the δ subunit (57).

We previously observed that residues 1-34 in Domain I undergo a local cooperative unfolding as they are deuterated faster and display EX1 kinetics in HXMS experiments (55, 56). The solvent accessibility of these residues signifies the greater flexibility in this region and suggests that β transiently opens in solution. The crystallographic data along with HXMS experiments suggest that the γ complex traps β in an open conformation as the strain held at the dimer interface is alleviated and the δ subunit serves to prevent ring closure. The δ subunit does not open β at the dimer interface but rather stabilizes one monomer, preventing ring closure. Here, we further investigate the dynamic behavior at the dimer interface and its effect on the opening and closing of the ring structure. Using the crystal structure of WT β as a guide we designed mutations with the intention of stabilizing or destabilizing the dimer interface.

The mutations we hypothesized to be stabilizing, T45R, T47R, S107R, and S109R, had similar or increased thermostability compared to WT β and similar functions as WT β except for having greater residence on DNA after loading (Fig. 8). The atomic fluctuations that the mutations

produced in the MD simulations were examined by performing RMSF analysis. The highest increase in the mobility of residues G209, G210, and D211 was observed in the T45R variant. The same residues on the opposite monomer were less mobile in all other variants except for the T47R variant. The hydrogen bond analysis of the MD simulations determined that residues R45 and R47 within T45R and T47R variants formed new interactions with E52 relative to WT β (Fig. S17). Additionally, in the S107R variant, R107 formed interactions with E93 (Fig. S20E). Lastly, R96 was observed to interact with Q299 and S107 in the S109R variant (Fig. S20). The mutations designed to be destabilizing disrupted the dimer interface to varying degrees (Fig. 8). The L82D variant by far produced the greatest destabilization effect and in comparison, L82E had milder effects. When the L82E mutation was combined with I272A the effect closely resembled the L82D variant. The β L82D and L82E I272A variants had significantly reduced thermostability; whereas β L82E moderately reduced the melting temperature of the protein by ~7 °C (Fig. 8). The dimerization state of all three variants was altered, with β L82D detected as a monomer at concentrations in the μM range, β L82E I272A as monomer and dimer, and β L82E as dimer and multimer by native PAGE and native TIMS-MS. The β L82D and β L82E I272A variants did not complement cell growth in the temperature sensitivity assay. The β L82E variant supported cell growth but resulted in smaller colonies that grew to a normal size with longer incubation time. The intrinsic ATPase activity of the clamp loader was not stimulated by the addition of β L82D, whereas β L82E and β L82E I272A stimulated the ATPase activity to nearly the same extent as the WT β clamp. The destabilized β L82E and β L82E I272A variants did not appear to unload from the linear, end-blocked DNA substrate. One possibility that would explain this observation is that these variants might remain bound to the γ complex as the δ subunit has been shown to have greater affinity for an open clamp. The L82E and L82E I272A variants had similar affinity for mini-δ as WT β, but those experiments were carried out only with mini-δ, whereas the clamp loading experiments were performed with the complete clamp loader complex and DNA. The β L82D variant did not stimulate the ATPase activity of the γ clamp loader and was loaded onto DNA less efficiently than WT β. The RMSF of L248, which is in close proximity to the β client protein-binding pocket (19, 57, 92), was observed to increase in one of the monomers in the L82E I272A variant. P20′, L21′, and G22′ on the second monomer were observed to be more mobile in the L82E variant. These residues are located on the complementary region consisting of residues 1-34, which was previously reported to undergo a local cooperative unfolding and to display EX1 kinetics in the HXMS experiments (55, 56). Difference cross-correlation analysis for these destabilizing variants suggests that at least one of the two dimer interfaces (both interfaces in L82D) exhibit higher anti-correlated movement in the interface region compared to WT β, as well as higher changes in correlation overall. The hydrogen bond analysis revealed that changing the leucine at the 82 position to either an aspartic acid or glutamic acid resulted in new interactions between D/E82 and R269 and between G81 and Q265. These new hydrogen bond interactions also reduce a contact between the G81 backbone and R269 sidechain in WT β. Taken together, the MD simulations suggest that the changes in specific hydrogen-bond contacts and other non-covalent interactions induced by the point mutations result in significant changes in conformation and dynamics that are consistent with the observed experimental results for both the stabilizing and destabilizing mutations.

Our rational approach resulted in variants with stabilizing and tunable destabilizing mutations which likely render the clamp closed or open, respectively. We also report here molecular dynamics simulations that rationalize our observations of the effects of these mutations on the biological activities of the resulting clamp variants, as well as the complete hydrogen bond

interaction map. We are now working to create stable monomers in solution by designing the next generation of mutations.

SUPPORTING MATERIAL

Supporting material is available.

AUTHOR CONTRIBUTIONS

BNK, HG, AAR, FF-L, DMK, GAC, and PJB designed research. BNK, HG, AAR, SL, KJDF, AC, and
MLL performed research and analyzed data. BNK, HG, AAR, SL, KJDF, FF-L, DMK, GAC, and PJB
wrote the manuscript.

ACKNOWLEDGEMENT

We thank Jane Compton for technical assistance and Heidi Erlandsen from the UConn Biophysics Core
for help with ITC.

FUNDING

This work was supported by the National Institutes of Health [R01GM123239 to P.J.B. and D.M.K.] and
the National Science Foundation [MCB-1615946 to P.J.B.; MCB-1615866 to D.M.K.; CHE-1654274 CAREER Award to F.F.L.]. Computing time from UNT CASCaM with support from NSF CHE-1531468
is gratefully acknowledged.

CONFLICT OF INTEREST

The authors declare no conflict of interest.

REFERENCES

1. Georgescu, R.E., S.S. Kim, O. Yurieva, J. Kuriyan, X.P. Kong, and M. O'Donnell 2008. Structure
of a sliding clamp on DNA. Cell. 132:43-54.
2. Sutton, M.D. 2010. Coordinating DNA polymerase traffic during high and low fidelity synthesis.
Biochim Biophys Acta. 1804:1167-1179.
3. Bloom, L.B., X. Chen, D.K. Fygenson, J. Turner, M. O'Donnell, and M.F. Goodman 1997. Fidelity of *Escherichia coli* DNA polymerase III holoenzyme. The effects of beta, gamma complex processivity proteins and epsilon proofreading exonuclease on nucleotide misincorporation efficiencies. J Biol Chem. 272:27919-27930.
4. Kong, X.P., R. Onrust, M. O'Donnell, and J. Kuriyan 1992. Three-dimensional structure of the beta subunit of *E. coli* DNA polymerase III holoenzyme: a sliding DNA clamp. Cell. 69:425-437.
5. Krishna, T.S.R., X.P. Kong, S. Gary, P.M. Burgers, and J. Kuriyan 1994. Crystal structure of the

eukaryotic DNA polymerase processivity factor PCNA. Cell. 79:1233-1243.
6. Williams, G.J., K. Johnson, J. Rudolf, S.A. McMahon, L. Carter, M. Oke, H. Liu, G.L. Taylor, M.F. White, and J.H. Naismith 2006. Structure of the heterotrimeric PCNA from *Sulfolobus solfataricus*. Acta Crystallogr Sect F Struct Biol Cryst Commun. 62:944-948.
7. Moarefi, I., D. Jeruzalmi, J. Turner, M. O'Donnell, and J. Kuriyan 2000. Crystal structure of the
DNA polymerase processivity factor of T4 bacteriophage. J Mol Biol. 296:1215-1223.
8. Oakley, A.J., P. Prosselkov, G. Wijffels, J.L. Beck, M.C. Wilce, and N.E. Dixon 2003. Flexibility
revealed by the 1.85 A crystal structure of the beta sliding-clamp subunit of *Escherichia coli* DNA polymerase III. Acta Crystallogr D Biol Crystallogr. 59:1192-1199.
9. Gulbis, J.M., Z. Kelman, J. Hurwitz, M. O'Donnell, and J. Kuriyan 1996. Structure of the Cterminal
region of p21-WAF1/CIP1 complexed with human PCNA. Cell. 87:297-306.
10. Wang, K., Z. Shi, M. Zhang, and D. Cheng 2013. Structure of PCNA from Drosophila melanogaster. Acta Crystallogr Sect F Struct Biol Cryst Commun. 69:387-392.
11. Matsumiya, S., Y. Ishino, and K. Morikawa 2001. Crystal structure of an archaeal DNA sliding
clamp: proliferating cell nuclear antigen from Pyrococcus furiosus. Protein Sci. 10:17-23.
12. Fay, P.J., K.O. Johanson, C.S. McHenry, and R.A. Bambara 1981. Size classes of products synthesized processively by DNA polymerase III and DNA polymerase III holoenzyme of *Escherichia coli*. J Biol Chem. 256:976-983.
13. Yao, N.Y., R.E. Georgescu, J. Finkelstein, and M.E. O'Donnell 2009. Single-molecule analysis
reveals that the lagging strand increases replisome processivity but slows replication fork progression. Proc Natl Acad Sci U S A. 106:13236-13241.
14. Maki, H. and A. Kornberg 1985. The polymerase subunit of DNA polymerase III of *Escherichia*
coli. II. Purification of the alpha subunit, devoid of nuclease activities. J Biol Chem. 260:12987-12992.
15. Maki, S. and A. Kornberg 1988. DNA polymerase III holoenzyme of *Escherichia coli*. II. A novel complex including the gamma subunit essential for processive synthesis. J Biol Chem. 263:6555-6560.
16. Lopez de Saro, F.J. and M. O'Donnell 2001. Interaction of the beta sliding cla17. Hughes, A.J., Jr., S.K. Bryan, H. Chen, R.E. Moses, and C.S. McHenry 1991. *Escherichia coli*
DNA polymerase II is stimulated by DNA polymerase III holoenzyme auxiliary subunits. J Biol Chem. 266:4568-4573.
18. Bonner, C.A., P.T. Stukenberg, M. Rajagopalan, R. Eritja, M. O'Donnell, K. McEntee, H. Echols,
and M.F. Goodman 1992. Processive DNA synthesis by DNA polymerase II mediated by DNA polymerase III accessory proteins. J Biol Chem. 267:11431-11438.
19. Dalrymple, B.P., K. Kongsuwan, G. Wijffels, N.E. Dixon, and P.A. Jennings 2001. A universal
protein-protein interaction motif in the eubacterial DNA replication and repair systems. Proc Natl
Acad Sci U S A. 98:11627-11632.

20. Stukenberg, P.T., P.S. Studwell-Vaughan, and M. O'Donnell 1991. Mechanism of the sliding beta-clamp of DNA polymerase III holoenzyme. J Biol Chem. 266:11328-11334.
21. Naktinis, V., J. Turner, and M. O'Donnell 1996. A molecular switch in a replication machine defined by an internal competition for protein rings. Cell. 84:137-145.
22. Wagner, J., S. Fujii, P. Gruz, T. Nohmi, and R.P. Fuchs 2000. The beta clamp targets DNA polymerase IV to DNA and strongly increases its processivity. EMBO Rep. 1:484-488.
23. Lenne-Samuel, N., J. Wagner, H. Etienne, and R.P. Fuchs 2002. The processivity factor beta controls DNA polymerase IV traffic during spontaneous mutagenesis and translesion synthesis *in vivo*. EMBO Rep. 3:45-49.
24. Tang, M., P. Pham, X. Shen, J.S. Taylor, M. O'Donnell, R. Woodgate, and M.F. Goodman 2000.
Roles of *E. coli* DNA polymerases IV and V in lesion-targeted and untargeted SOS mutagenesis. Nature. 404:1014-1018.
25. Tang, M., X. Shen, E.G. Frank, M. O'Donnell, R. Woodgate, and M.F. Goodman 1999. UmuD'(2)C is an error-prone DNA polymerase, *Escherichia coli* pol V. Proc Natl Acad Sci U S A. 96:8919-8924.
26. Bunting, K.A., S.M. Roe, and L.H. Pearl 2003. Structural basis for recruitment of translesion DNA polymerase pol IV/DinB to the beta-clamp. EMBO J. 22:5883-5892.
27. Indiani, C., P. McInerney, R. Georgescu, M.F. Goodman, and M. O'Donnell 2005. A slidingclamp
toolbelt binds high- and low-fidelity DNA polymerases simultaneously. Mol Cell 19:805-815.
28. Kath, J.E., S. Jergic, J.M. Heltzel, D.T. Jacob, N.E. Dixon, M.D. Sutton, G.C. Walker, and J.J.
Loparo 2014. Polymerase exchange on single DNA molecules reveals processivity clamp control of translesion synthesis. Proc Natl Acad Sci U S A. 111:7647–7652.
29. Kath, J.E., S. Chang, M.K. Scotland, J.H. Wilbertz, S. Jergic, N.E. Dixon, M.D. Sutton, and J.J.
Loparo 2016. Exchange between *Escherichia coli* polymerases II and III on a processivity clamp.
Nucleic Acids Res. 44:1681-1690.
30. Katayama, T., T. Kubota, K. Kurokawa, E. Crooke, and K. Sekimizu 1998. The initiator function
of DnaA protein is negatively regulated by the sliding clamp of the *E. coli* chromosomal replicase.
Cell. 94:61-71.
31. Kurz, M., B. Dalrymple, G. Wijffels, and K. Kongsuwan 2004. Interaction of the sliding clamp
beta-subunit and Hda, a DnaA-related protein. J Bacteriol. 186:3508-3515.
32. Beyer, A. 1997. Sequence analysis of the AAA protein family. Protein Sci. 6:2043-2058.
33. Hedglin, M., R. Kumar, and S.J. Benkovic 2013. Replication Clamps and Clamp Loaders. Cold
Spring Harbor Perspectives in Biology. 5.
34. Kelch, B.A. 2016. Review: The lord of the rings: Structure and mechanism of the sliding clamp
loader. Biopolymers. 105:532-546.

35. Kelch, B.A., D.L. Makino, M. O'Donnell, and J. Kuriyan 2012. Clamp loader ATPases and the
evolution of DNA replication machinery. BMC Biol. 10:34.
36. Marzahn, M.R., J.N. Hayner, J. Finkelstein, M. O'Donnell, and L.B. Bloom 2014. The ATP sites
of AAA+ clamp loaders work together as a switch to assemble clamps on DNA. J Biol Chem. 289:5537-5548.
37. Goedken, E.R., M. Levitus, A. Johnson, C. Bustamante, M. O'Donnell, and J. Kuriyan 2004. Fluorescence measurements on the *E.coli* DNA polymerase clamp loader: implications for conformational changes during ATP and clamp binding. J Mol Biol. 336:1047-1059.
38. Kazmirski, S.L., M. Podobnik, T.F. Weitze, M. O'Donnell, and J. Kuriyan 2004. Structural analysis of the inactive state of the *Escherichia coli* DNA polymerase clamp-loader complex. Proc Natl Acad Sci U S A. 101:16750-16755.
39. Paschall, C.O., J.A. Thompson, M.R. Marzahn, A. Chiraniya, J.N. Hayner, M. O'Donnell, A.H.
Robbins, R. McKenna, and L.B. Bloom 2011. The *Escherichia coli* clamp loader can actively pry
open the beta-sliding clamp. J Biol Chem. 286:42704-42714.
40. Jeruzalmi, D., M. O'Donnell, and J. Kuriyan 2001. Crystal structure of the processivity clamp loader gamma (gamma) complex of *E. coli* DNA polymerase III. Cell. 106:429-441.
41. Simonetta, K.R., S.L. Kazmirski, E.R. Goedken, A.J. Cantor, B.A. Kelch, R. McNally, S.N. Seyedin, D.L. Makino, M. O'Donnell, and J. Kuriyan 2009. The mechanism of ATP-dependent primer-template recognition by a clamp loader complex. Cell. 137:659-671.
42. Yao, N., J. Turner, Z. Kelman, P.T. Stukenberg, F. Dean, D. Shechter, Z.Q. Pan, J. Hurwitz, and
M. ODonnell 1996. Clamp loading, unloading and intrinsic stability of the PCNA, beta and gp45 sliding clamps of human, *E-coli* and T4 replicases. Genes to Cells. 1:101-113.
43. Soumillion, P., D.J. Sexton, and S.J. Benkovic 1998. Clamp subunit dissociation dictates bacteriophage T4 DNA polymerase holoenzyme disassembly. Biochemistry. 37:1819-1827.
44. Alley, S.C., V.K. Shier, E. Abel-Santos, D.J. Sexton, P. Soumillion, and S.J. Benkovic 1999. Sliding clamp of the bacteriophage T4 polymerase has open and closed subunit interfaces in solution. Biochemistry. 38:7696-7709.
45. Millar, D., M.A. Trakselis, and S.J. Benkovic 2004. On the solution structure of the T4 sliding
clamp (gp45). Biochemistry. 43:12723-12727.
46. Trakselis, M.A., S.C. Alley, E. Abel-Santos, and S.J. Benkovic 2001. Creating a dynamic picture
of the sliding clamp during T4 DNA polymerase holoenzyme assembly by using fluorescence resonance energy transfer. Proc Natl Acad Sci U S A. 98:8368-8375.
47. Gadkari, V.V., S.R. Harvey, A.T. Raper, W.T. Chu, J. Wang, V.H. Wysocki, and Z. Suo 2018.
Investigation of sliding DNA clamp dynamics by single-molecule fluorescence, mass spectrometry and structure-based modeling. Nucleic Acids Res. 46:3103-3118.
48. De Biasio, A., R. Sanchez, J. Prieto, M. Villate, R. Campos-Olivas, and F.J. Blanco 2011. Reduced stability and increased dynamics in the human proliferating cell nuclear antigen (PCNA)

relative to the yeast homolog. PLoS One. 6:e16600.
49. Chen, S., M.K. Levin, M. Sakato, Y. Zhou, and M.M. Hingorani 2009. Mechanism of ATPdriven
PCNA clamp loading by *S. cerevisiae* RFC. J Mol Biol. 388:431-442.
50. Thompson, J.A., M.R. Marzahn, M. O'Donnell, and L.B. Bloom 2012. Replication factor C is a
more effective proliferating cell nuclear antigen (PCNA) opener than the checkpoint clamp loader,
Rad24-RFC. J Biol Chem. 287:2203-2209.
51. Sakato, M., Y. Zhou, and M.M. Hingorani 2012. ATP binding and hydrolysis-driven ratedetermining
events in the RFC-catalyzed PCNA clamp loading reaction. J Mol Biol. 416:176-191.
52. Binder, J.K., L.G. Douma, S. Ranjit, D.M. Kanno, M. Chakraborty, L.B. Bloom, and M. Levitus
2014. Intrinsic stability and oligomerization dynamics of DNA processivity clamps. Nucleic Acids Res. 42:6476-6486.
53. Tainer, J.A., J.A. McCammon, and I. Ivanov 2010. Recognition of the ring-opened state of proliferating cell nuclear antigen by replication factor C promotes eukaryotic clamp-loading. J Am Chem Soc. 132:7372-7378.
54. Purohit, A., J.K. England, L.G. Douma, F. Tondnevis, L.B. Bloom, and M. Levitus 2017. Electrostatic interactions at the dimer interface stabilize the *E. coli* beta sliding clamp. Biophys J. 113:794-804.
55. Fang, J., J.R. Engen, and P.J. Beuning 2011. *Escherichia coli* processivity clamp beta from DNA
polymerase III is dynamic in solution. Biochemistry. 50:5958-5968.
56. Fang, J., P. Nevin, V. Kairys, C. Venclovas, J.R. Engen, and P.J. Beuning 2014. Conformational
analysis of processivity clamps in solution demonstrates that tertiary structure does not correlate with protein dynamics. Structure. 22:572-581.
57. Jeruzalmi, D., O. Yurieva, Y. Zhao, M. Young, J. Stewart, M. Hingorani, M. O'Donnell, and J.
Kuriyan 2001. Mechanism of processivity clamp opening by the delta subunit wrench of the clamp loader complex of *E. coli* DNA polymerase III. Cell. 106:417-428.
58. Oakley, A.J. 2016. Dynamics of Open DNA Sliding Clamps. PLoS One. 11:e0154899.
59. Leu, F.P., M.M. Hingorani, J. Turner, and M. O'Donnell 2000. The delta subunit of DNA polymerase III holoenzyme serves as a sliding clamp unloader in *Escherichia coli*. J Biol Chem. 275:34609-34618.
60. Alyami, E.M., A.A. Rizzo, P.J. Beuning, and D.M. Korzhnev 2017. NMR resonance assignments
for the N-terminal domain of the delta subunit of the *E. coli* gamma clamp loader complex. Biomol NMR Assign. 11:169-173.
61. Erster, O. and M. Liscovitch 2010. A modified inverse PCR procedure for insertion, deletion, or
replacement of a DNA fragment in a target sequence and its application in the ligand interaction scan method for generation of ligand-regulated proteins. Methods Mol. Biol. 634:157-174.

62. Heltzel, J.M., S.K. Scouten Ponticelli, L.H. Sanders, J.M. Duzen, V. Cody, J. Pace, E.H. Snell,
and M.D. Sutton 2009. Sliding clamp-DNA interactions are required for viability and contribute to DNA polymerase management in *Escherichia coli*. J Mol Biol. 387:74-91.
63. Bianco, P.R., S. Pottinger, H.Y. Tan, T. Nguyenduc, K. Rex, and U. Varshney 2017. The IDL of
E. coli SSB links ssDNA and protein binding by mediating protein-protein interactions. Protein Sci. 26:227-241.
64. Yu, C., H.Y. Tan, M. Choi, A.J. Stanenas, A.K. Byrd, K.D. Raney, C.S. Cohan, and P.R. Bianco
2016. SSB binds to the RecG and PriA helicases *in vivo* in the absence of DNA. Genes to Cells. 21:163-184.
65. Ericsson, U.B., B.M. Hallberg, G.T. Detitta, N. Dekker, and P. Nordlund 2006. Thermofluorbased
high-throughput stability optimization of proteins for structural studies. Anal Biochem. 357:289-298.
66. Fernandez-Lima, F., D.A. Kaplan, J. Suetering, and M.A. Park 2011. Gas-phase separation using
a trapped ion mobility spectrometer. Int J Ion Mobil Spectrom. 14.
67. Fernandez-Lima, F.A., D.A. Kaplan, and M.A. Park 2011. Note: Integration of trapped ion mobility spectrometry with mass spectrometry. Rev Sci Instrum. 82:126106.
68. McDaniel, E.W. and E.A. Mason (1973), *Mobility and diffusion of ions in gases*. New York, NY:
John Wiley and Sons, Inc.
69. Hernandez, D.R., J.D. Debord, M.E. Ridgeway, D.A. Kaplan, M.A. Park, and F. Fernandez-Lima
2014. Ion dynamics in a trapped ion mobility spectrometer. Analyst. 139:1913-1921.
70. Sutton, M.D., J.M. Duzen, and R.W. Maul 2005. Mutant forms of the *Escherichia coli* beta sliding clamp that distinguish between its roles in replication and DNA polymerase V-dependent translesion DNA synthesis. Mol Microbiol. 55:1751-1766.
71. Sambrook, J., E.F. Fritsch, and T. Maniatis (1989), *Molecular Cloning: a laboratory manual*. Cold Spring Harbor, NY: Cold Spring Harbor Laboratory Press.
72. Parasuram, R., T.A. Coulther, J.M. Hollander, E. Keston-Smith, M.J. Ondrechen, and P.J. Beuning 2018. Prediction of Active Site and Distal Residues in E. coli DNA Polymerase III alpha
Polymerase Activity. Biochemistry. 57:1063-1072.
73. Case, D.A., Cerutti, D. S., T.E. Cheatham, III, T.A. Darden, R.E. Duke, T.J. Giese, Gohlke, H.,
A.W. Goetz, D. Greene, N. Homeyer, S. Izadi, A. Kovalenko, T. Lee, S., S. LeGrand, P. Li, C. Lin, J. Liu, T. Luchko, R. Luo, Mermelstein, D., K.M. Merz, G. Monard, H. Nguyen, I. Omelyan,
A. Onufriev, F. Pan, R. Qi, D.R. Roe, A. Roitberg, C. Sagui, C.L. Simmerling, Botello-Smith, W.
M., J. Swails, R.C. Walker, J. Wang, R.M. Wolf, X. Wu, L. Xiao, York, D. M., and P.A. Kollman,
AMBER 2017. 2017, University of California: San Francisco.

74. Maier, J.A., C. Martinez, K. Kasavajhala, L. Wickstrom, K.E. Hauser, and C. Simmerling 2015.
ff14SB: Improving the accuracy of protein side chain and backbone parameters from ff99SB. J Chem Theory Comput. 11:3696-3713.
75. Gotz, A.W., M.J. Williamson, D. Xu, D. Poole, S. Le Grand, and R.C. Walker 2012. Routine microsecond molecular dynamics simulations with AMBER on GPUs. 1. generalized born. J Chem Theory Comput. 8:1542-1555.
76. Le Grand, S., A.W. Gotz, and R.C. Walker 2013. SPFP: speed without compromise-a mixed precision model for GPU accelerated molecular dynamics simulations. Computer Physics Communications. 184:374-380.
77. Berendsen, H.J.C., J.P.M. Postma, W.F. van Gunsteren, A. DiNola, and J.R. Haak 1984. Molecular dynamics with coupling to an external bath. J Chem Phys. 81:3684-3690.
78. Essmann, U., L. Perera, M.L. Berkowitz, T. Darden, H. Lee, and L.G. Pedersen 1995. A smooth
particle mesh Ewald method. J Chem Phys. 103:8577-8593.
79. Roe, D.R. and T.E. Cheatham 2013. PTRAJ and CPPTRAJ: software for processing and analysis
of molecular dynamics trajectory data. J Chem Theory Comput. 9:3084-3095.
80. Humphrey, W., A. Dalke, and K. Schulten 1996. VMD: visual molecular dynamics. J Mol Graph.
14:33-38, 27-38.
81. MarvinSketch. *v17.26.0, developed by ChemAxon* 2017; Available from: http://www.chemaxon.com.
82. Stewart, J., M.M. Hingorani, Z. Kelman, and M. O'Donnell 2001. Mechanism of beta clamp opening by the delta subunit of *Escherichia coli* DNA polymerase III holoenzyme. J Biol Chem. 276:19182-19189.
83. Bertram, J.G., L.B. Bloom, J. Turner, M. O'Donnell, J.M. Beechem, and M.F. Goodman 1998.
Pre-steady state analysis of the assembly of wild type and mutant circular clamps of *Escherichia coli* DNA polymerase III onto DNA. J Biol Chem. 273:24564-24574.
84. Simonetta, K.R., *Structural Studies of the Mechanism of Clamp Loading by Clamp Loader Complexes*, in *Molecular and Cell Biology*. 2010, University of California, Berkeley, Ph.D. Dissertation.
85. Beuning, P.J., D. Sawicka, D. Barsky, and G.C. Walker 2006. Two processivity clamp interactions differentially alter the dual activities of UmuC. Mol Microbiol. 59:460-474.
86. Heltzel, J., R. Maul, S. Scouten Ponticelli, and M. Sutton 2009. A model for DNA polymerase
switching involving a single cleft and the rim of the sliding clamp. Proc Natl Acad Sci U S A. 106:12664-12669.
87. Scouten Ponticelli, S.K., J.M. Duzen, and M.D. Sutton 2009. Contributions of the individual hydrophobic clefts of the *Escherichia coli* beta sliding clamp to clamp loading, DNA replication and clamp recycling. Nucleic Acids Res. 37:2796-2809.
88. Park, M.S. and M. O'Donnell 2009. The clamp loader assembles the beta clamp onto either a 3' or
5' primer terminus: the underlying basis favoring 3' loading. J Biol Chem. 284:31473-31483.

89. Kelch, B.A., D.L. Makino, M. O'Donnell, and J. Kuriyan 2011. How a DNA polymerase clamp
loader opens a sliding clamp. Science. 334:1675-1680.
90. Bowman, G.D., M. O'Donnell, and J. Kuriyan 2004. Structural analysis of a eukaryotic sliding
DNA clamp-clamp loader complex. Nature. 429:724-730.
91. Naktinis, V., R. Onrust, L. Fang, and M. O'Donnell 1995. Assembly of a chromosomal replication machine: two DNA polymerases, a clamp loader, and sliding clamps in one holoenzyme particle. II. Intermediate complex between the clamp loader and its clamp. J Biol Chem. 270:13358-13365.
92. Burnouf, D.Y., V. Olieric, J. Wagner, S. Fujii, J. Reinbolt, R.P. Fuchs, and P. Dumas 2004. Structural and biochemical analysis of sliding clamp/ligand interactions suggest a competition between replicative and translesion DNA polymerases. J Mol Biol. 335:1187-1197.

Table 1. Binding parameters for mini-δ and β-clamp variants obtained by ITC

β-clamp variant	K_D (μM)	n	ΔH (kJ/mol)	ΔS (J/mol/K)	T (°C)
WT	5.6 ± 0.69	1.01 ± 2.0x10^{-4}	-21.6 ± 0.4	27.7	25
I272A L273A	0.53 ± 0.08	0.71 ± 0.01	-34.6 ± 0.4	2.0	20
L82E	6.6 ± 1.8	0.83 ± 0.03	-17.8 ± 1.1	38.6	20
L82E I272A	5.5 ± 1.0	0.41 ± 0.01	-34.0 ± 2.0	-15.3	20
S107R	4.4 ± 0.9	0.96 ± 0.02	-20.4 ± 0.8	34.2	25
S109R	5.0 ± 1.1	1.06 ± 0.03	-19.4 ± 0.9	36.5	25
T45R	6.7 ± 2.0	0.95 ± 0.03	-22.5 ± 1.5	23.4	25
T47R	6.0 ± 1.7	0.95 ± 0.03	-22.5 ± 1.4	24.3	25

Mini-δ (0.6-0.7 mM) was titrated into 0.1 mM β-clamp solution. The parameters include the dissociation constant K_D, association enthalpy ΔH, binding stoichiometry parameter n, and association entropy ΔS obtained at 25 °C (20 °C for L82E, L82E I272A, and I272A/L273A β variants).

FIGURE LEGENDS

Figure 1. Design of β clamp mutations to stabilize or destabilize the dimer interface. Monomer A is depicted in gray and Monomer B is depicted in purple on the three-dimensional representations. The locations of mutations in Domain I (T45 and T47 variants) are depicted with blue beads while the mutations at the dimer interface (L82D, L82E, L82E I 272A, S107R and S109R variants) are depicted with green beads on the protein.

Figure 2. Differential scanning fluorimetry of WT and variant β clamps. Melting temperatures observed by monitoring Sypro Orange dye fluorescence. Bar graph showing average melting temperatures and standard deviations for WT β (light blue), β T45R (red), β T47R (green), β S107R (purple), β S109R (cyan), β L82D (orange), β L82E (dark blue), and β L82E I272A (maroon) from triplicate experiments.

Figure 3. Native gel electrophoresis to assess dimerization state of variants. (**A**) denaturing PAGE showing purified WT and variant clamp proteins as monomers in the presence of SDS. (**B**) native PAGE shows monomeric (mono), dimeric (di), multimeric (multi) conformations of WT and variant clamp proteins at 1 μg each.

Figure 4. MS and TIMS spectra for the multiply protonated species of the β clamp (**A**) WT, (**B**) L82E, (**C**) L82E I272A and (**D**) L82D variants. (**E**) The distribution of monomers:dimers:tetramers (Table S1).

Figure 5. ATPase activity of the γ complex measured using a BIOMOL® Green colorimetric reagent. (**A**) a schematic depicting loading of the β clamp onto a primer:template DNA with biotinylated 5′-ends. The template is longer than the primer resulting in a 3′ recessed end onto which the γ complex loads β in the presence of ATP. ATP hydrolysis ejects the clamp loader. The increase of inorganic phosphate following the loading reaction is measured by addition of the BIOMOL® Green reagent. (**B**) Bar graph showing the amount of phosphate released (nmol) during the loading reaction after the intrinsic γ complex ATPase activity is subtracted (γ complex hydrolyzes ATP in the presence of DNA, β enhances the ATPase activity of the γ complex). (**C**)

Immunoblot detection of β loaded onto a primer-template substrate using a bead-based assay for WT β and the variants indicated. Input control (L) indicates the amount of β in each loading reaction. After three wash steps (W1, W2, and W3), Pellet (P) fractions indicate loaded β and supernatant (S) fractions indicate unloaded β, respectively, for both 0- and 60-min time points (also see Fig. S3)

Figure 6. Ratio of colony forming units (cfu) at 37 °C vs. 30 °C for WT and variant β clamps in complementation assay. EV indicates the empty vector. Data represent the average and error bars represent the standard deviation of at least three replicates.

Figure 7. The total fraction of the frames that a hydrogen bond exists between (**A**) the backbone oxygen atom of G81 and side chain Q265′ (solid brown), and the backbone oxygen atom of G81′ and side chain Q265 (pattern brown); (**B**) the backbone oxygen atom of G81 and side chain R269′ (solid blue), and the backbone oxygen atom of G81′ and side chain R269 (pattern blue); (**C**) the side chain of D82/E82 and side chain R269′ (solid cyan), and the side chain of D/E82′ and side chain R269 (pattern cyan). The backbone oxygen atoms are depicted with subscript "O" while the side chain is depicted with subscript "SC." (**D**) The three-dimensional representation of the depicted interactions obtained from the trajectory at 85 ns of variant L82E I272A.

Figure 8. Summary of results presented, showing the different effects of each of the mutations made.

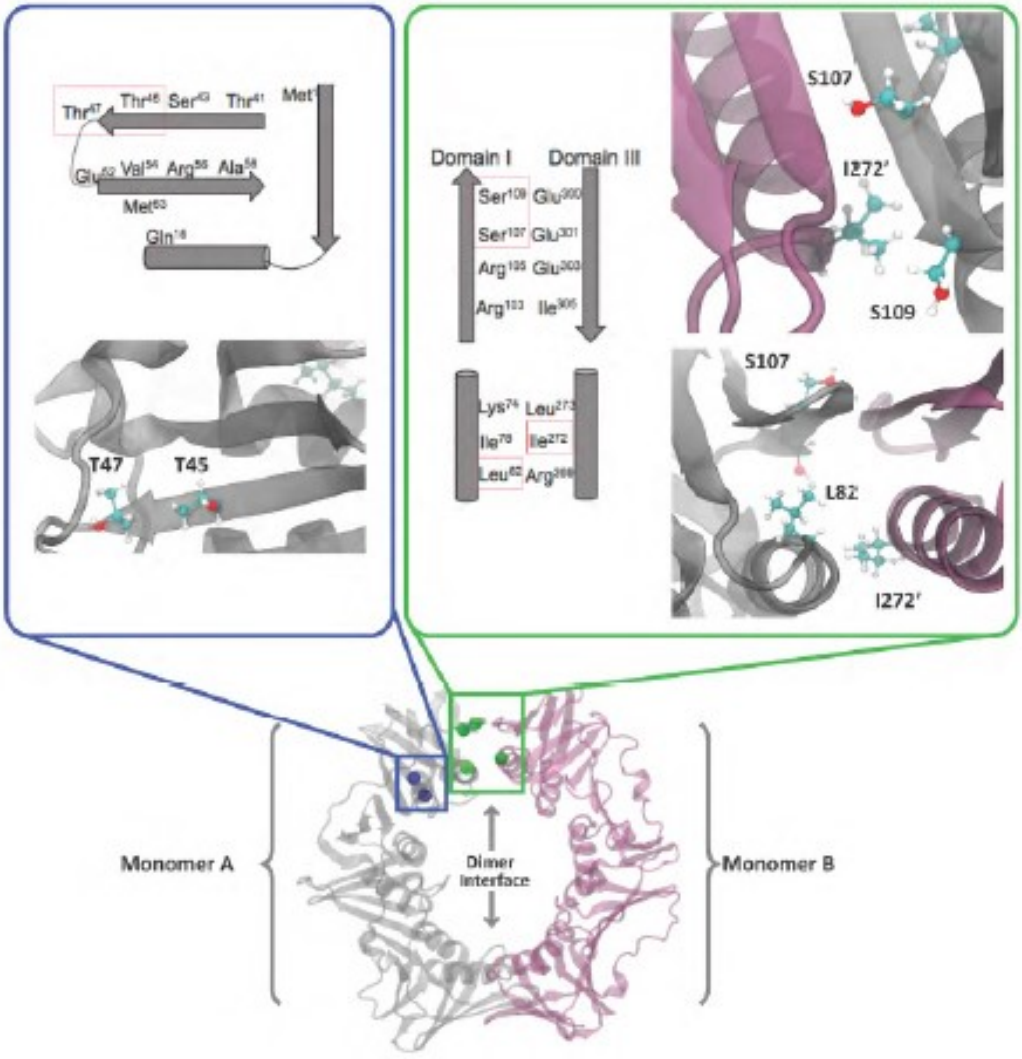
T47
T45
Domain I
Domain III
S107
I272'
S109
S107
L82
I272'
Monomer A
Dimer Interface
Monomer B

Figure 1.

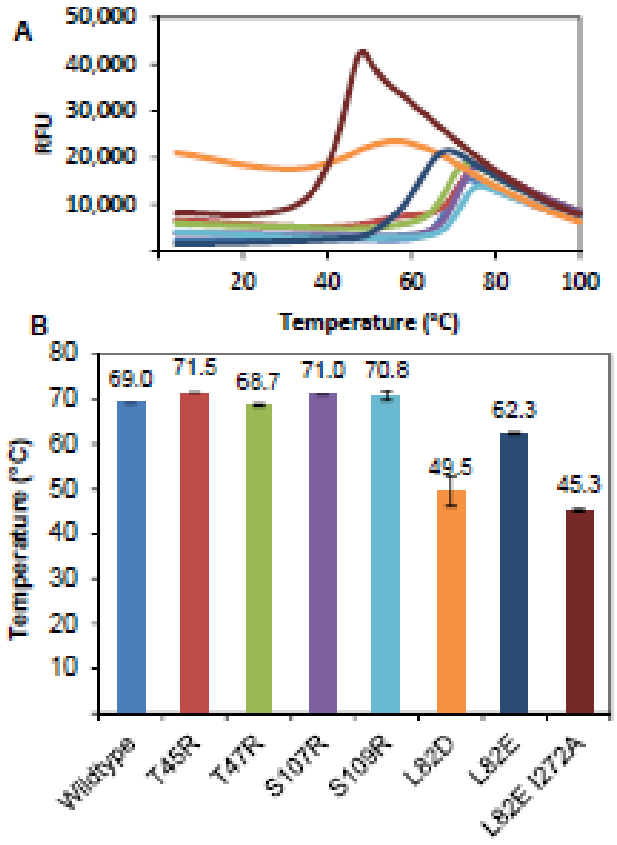
A
50,000
40,000
30,000
20,000
10,000
RFU
20
40
60
80
100
Temperature (°C)
B
80
70
60
50
40
30
20
10
Temperature (°C)
69.0
71.5
68.7
71.0
70.8
49.5
62.3
45.3
Wildtype
T45R
T47R
S107R
S109R
L82D
L82E
L82E I272A

Figure 2.

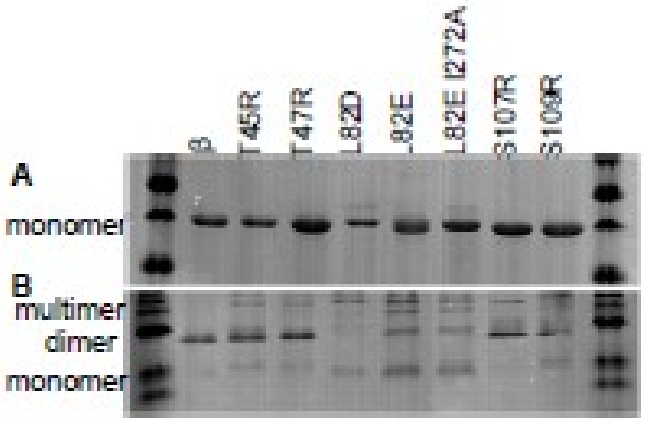
WT
T45R
T47R
L82D
L82E
L82E I272A
S107R
S108R
A
monomer
B
multimer
dimer
monomer

Figure 3.

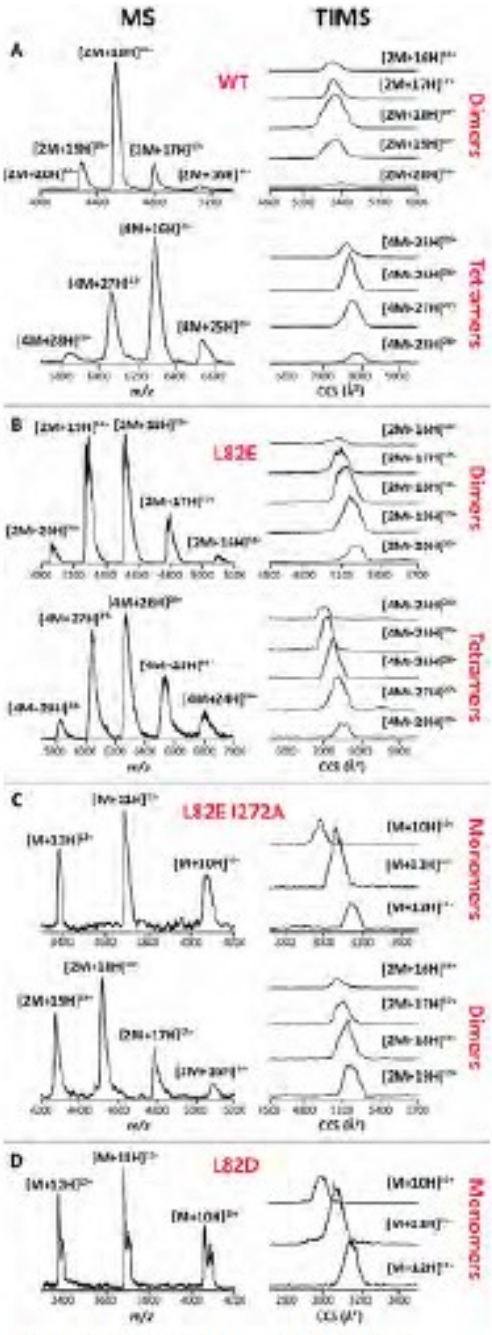

E

Clamp variant	N-mer Ratio
WT	0/6/1
L82E	0/3/1
L82E/I272A	1/1/0
L82D	1/0/0

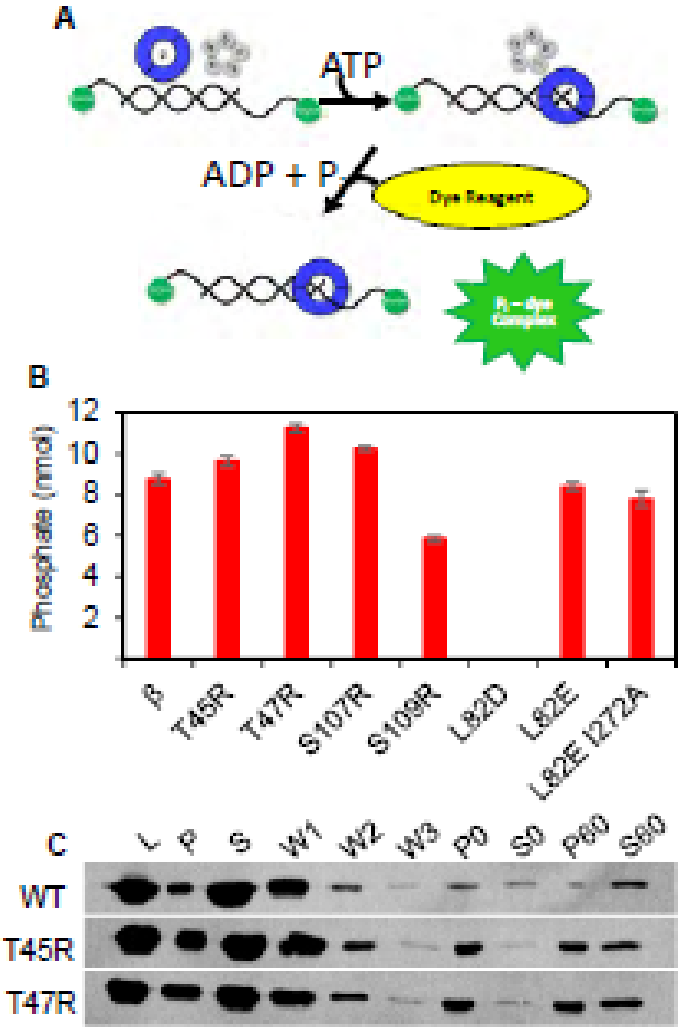
A
ATP
ADP + P
Dye Reagent
P–dye Complex
B
Phosphate (nmol)
12
10
8
6
4
2
P
T45R
T47R
S107R
S109R
L82D
L82E
L82E I272A
C
L
P
S
W1
W2
W3
P0
S0
P60
S60
WT
T45R
T47R

Figure 5.

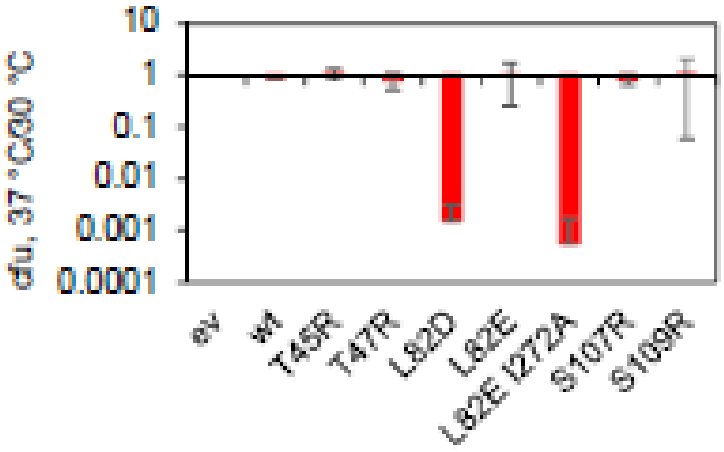
10
1
0.1
0.01
0.001
0.0001
cfu, 37 °C/30 °C
ev
wt
T45R
T47R
L82D
L82E
L82E I272A
S107R
S109R

Figure 6.

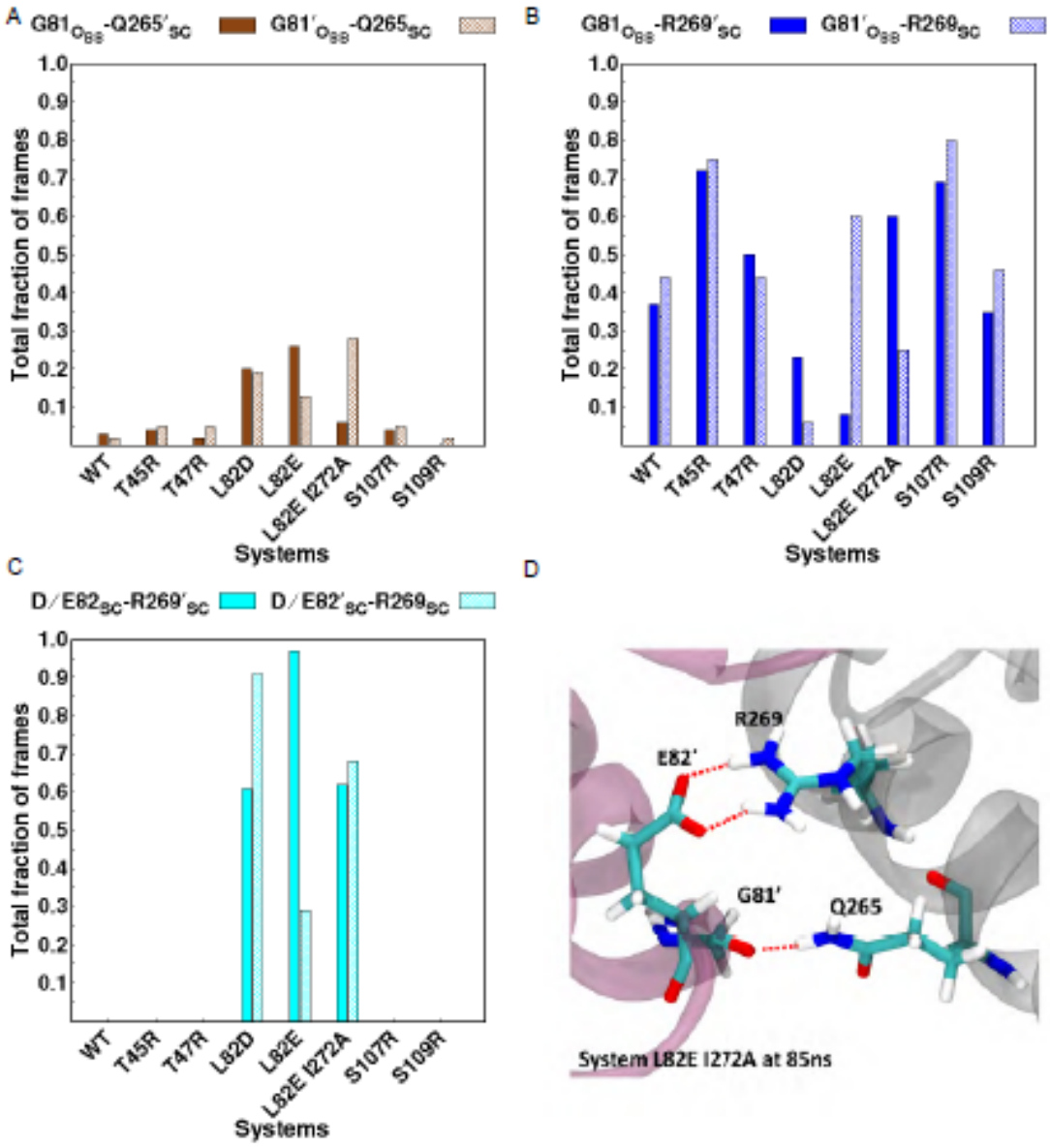
A
G81 Oδδ-Q265′ sc
G81′ Oδδ-Q265 sc
Total fraction of frames
1.0
0.9
0.8
0.7
0.6
0.5
0.4
0.3
0.2
0.1
WT
T45R
T47R
L82D
L82E
L82E I272A
S107R
S109R
Systems
B
G81 Oδδ-R269′ sc
G81′ Oδδ-R269 sc
Total fraction of frames
Systems
C
D/E82 sc-R269′ sc
D/E82′ sc-R269 sc
Total fraction of frames
Systems
D
R269
E82′
G81′
Q265
System L82E I272A at 85ns

Figure 7.

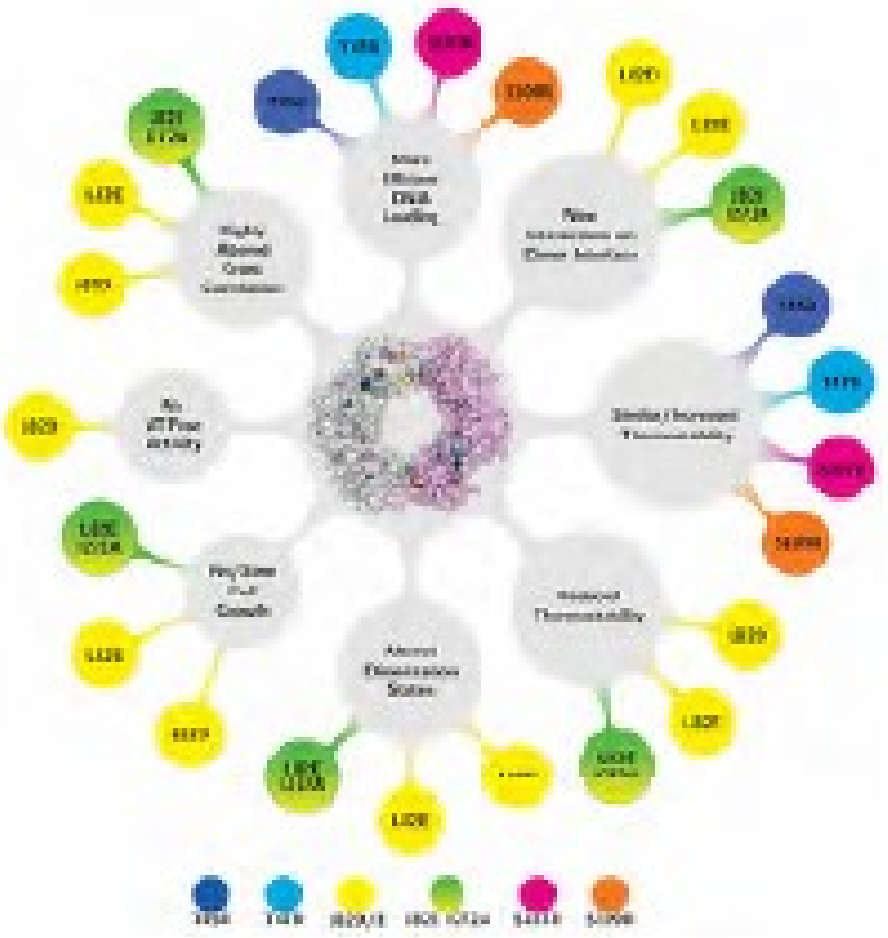

Figure 8.